Final Draft

of the original manuscript

Deng, M.; Wang, L.; Höche, D.; Lamaka, S.; Jiang, P.; Snihirova, D.; Scharnagl, N.; Zheludkevich, M.:

Ca/In micro alloying as a novel strategy to simultaneously enhance power and energy density of primary Mg-air batteries from anode aspect.

In: Journal of Power Sources. Vol. 472 (2020) 228528.

First published online by Elsevier: 07.07.2020

https://dx.doi.org/10.1016/j.jpowsour.2020.228528

Ca/In micro alloying as a novel strategy to simultaneously enhance power and energy density of primary Mg-air batteries from anode aspect

Min Deng[a,*], Linqian Wang[a], Daniel Höche[a, b], Sviatlana V. Lamaka[a], Pingli Jiang[a], Darya Snihirova[a], Nico Scharnagl[a], Mikhail L. Zheludkevich [a, c]

[a] *MagIC – Magnesium Innovation Centre, Helmholtz-Zentrum Geesthacht (HZG), 21502 Geesthacht, Germany*

[b] *Computational Material Design, Faculty of Mechanical Engineering, Helmut-Schmidt-University University of the Federal Armed Forces, 22043 Hamburg, Germany*

[c] *Institute of Materials Science, Faculty of Engineering, Kiel University, 24143 Kiel, Germany*

ABSTRACT: Herein we report micro-alloying with the combination of Ca/In as a novel strategy to improve the anode performance for Mg-air batteries. Two micro-alloyed Mg-Ca-In anodes, i.e. Mg-0.1%Ca-0.2%In and Mg-0.2%Ca-0.4%In (wt.%), are fabricated and evaluated in both configurations: half-cell and Mg-air full cell. Re-deposition of metallic In on anode surface during discharge is demonstrated. Anodic activation is then promoted by galvanic coupling between Mg and the re-deposited In, and film breakdown induced by In re-precipitation at the substrate/oxide film interface. Thus, the voltage and power density of Mg-air system are enhanced via adopting Mg-Ca-In anodes. Besides, wasteful-discharge of the Ca/In micro-alloyed anodes, which is related to the negative difference effect (NDE), is significantly suppressed. Anodic efficiency is consequently improved, reaching 80.2% at 5 mA cm^{-2} initial current density, and so is the service life of the Mg-air battery. Due to the enhanced voltage and anodic efficiency, Mg-Ca-In anodes enable Mg-air battery to exhibit outstanding energy density, e.g. 2259 Wh kg^{-1} at 5 mA cm^{-2}. Mg-0.1%Ca-0.2%In anode possesses superior performance in terms of low wasteful-discharge, enhanced discharge activity and high anodic efficiency. Therefore, we recommend micro-alloyed Mg-Ca-In, like Mg-0.1%Ca-0.2%In, as excellent candidates for anode materials of primary aqueous Mg-air batteries.

KEYWORDS: Mg-air batteries; Micro-alloying; Mg-Ca-In anodes; Discharge activity; Anodic efficiency.

* Corresponding author.
E-mail address: Min.Deng@hzg.de (M. Deng), Telephone number: +49 (0)4152 871936, Postal address: Helmholtz-Zentrum Geesthacht, Max-Planck-Str. 1, 21502 Geesthacht, Germany.

1. INTRODUCTION

The power sources with high energy density, high capacity, good stability and low cost are highly required. The investigation and development of rechargeable batteries attract much social attention due to their ability of recharging for many times, which results in a much lower cost of ownership than primary batteries. However, it is worth noting that rechargeable batteries are not applicable in some cases, such as in some places where recharging is impossible or impractical, like in the ocean or remote mountains. Primary batteries, under such circumstances, are better choices instead of rechargeable batteries because of their long self-life and high energy density [1, 2]. Besides, primary batteries are also important as backup power sources, for schools, hospitals, etc. Therefore, much effort should also be paid to search for economically feasible primary batteries with no hazard to the environment. Primary Mg-air batteries are promising power sources attributed to the good theoretical electrochemical properties of Mg metal, like the large volumetric capacity (3832 mA h cm^{-3} versus 2061 mA h cm^{-3} of Li) and relatively negative electrode potential (− 2.37 V vs. SHE) [3-6]. Besides, the adoption of oxygen from air as cathodic reactant reduces total weight of the battery system and, thus, remarkably enhances the energy density. Generally, the electrolytes used in primary Mg-air batteries are simple saline solutions with additives or natural seawater directly from the ocean [7-10]. Therefore, all components in this battery system are nonhazardous to the nature, rendering it a kind of environmentally benign energy system meeting the social requirement for green energy. In addition, the produced hydrogen gas accompanying the discharge process of Mg anode can also be the fuel source for fuel cells [11]. However, wide commercialization of primary Mg-air batteries is not yet achieved because of the insufficient practical properties. The rapid self-corrosion (or wasteful anode discharge) of Mg anodes during discharge leads to a shortened service life and reduced energy density of Mg-based battery system, due to the well-known negative difference effect (NDE) on Mg [12-14]. Besides, the battery voltage is relatively low because of the high open circuit potential (OCP, typically 1 V more positive than the theoretical thermodynamic potential) of ordinary Mg anode and large overpotential caused by sluggish anodic reaction kinetics or dense discharge products on anode surface [15-19]. Therefore, searching for Mg anode with low wasteful-discharge rate, more negative OCP and low anodic

overpotential is vital for the improvement of Mg-air batteries.

Alloying as a conventional approach is effective to improve various properties of Mg via controllable microstructure and chemical composition. Likewise, some alloying elements, like Al, Zn, Pb, Sn, In, Li and RE [17, 20-25], have been evaluated in attempt to modify the corrosion and discharge performance of Mg-based anode materials. Improvement has been achieved by an alloy with composition of Mg -11 wt.%Li -3 wt.%Al -1 wt.%Zn -0.2 wt.%Y, as reported by Liu et al. [20]. The voltage of a Mg-air battery with this Mg alloy as anode at 10 mA cm^{-2} in 3.5 wt.% NaCl electrolyte reaches around 1.32 V and the discharge capacity is approximately 1300 mA h g^{-1}. Apart from these, Mg-Hg alloys also attract interests as anode materials as they possess the most negative OCP among all Mg alloys as found [26-28]. As reported by Feng et al. [26], Mg-6 wt.% Hg alloy exhibits extremely negative corrosion potential in 3.5 wt.% NaCl solution (around – 2.2 V vs. SCE), which, in fact, is the most negative corrosion potential reported of any Mg alloy. Nevertheless, the usage of toxic elements, like Hg and Pb, is against the vital social requirement for green energy. It should also be noted that most research work focuses on Mg anode development via high content of alloying elements. The heavy alloying load results in high fraction of second phases and, therefore, leads to severe exfoliation of undissolved metallic pieces during discharge, which is normally termed as chunk effect (CE). As reported by Deng et al. [29], large loss of anodic efficiency (up to 50%) could be arisen from the occurrence of CE that is induced by preferential dissolution of Mg matrix surrounding the noble second phases. Consequently, the energy density of Mg-air system is reduced and the service life is decreased. In such cases, development of micro-alloyed Mg anodes is a feasible strategy to avoid this issue. Micro-alloyed Mg anodes with excellent discharge properties are highly required. Besides, it is noteworthy that Mg anodes should have low wasteful-discharge rate during discharge to obtain high anodic efficiency and, consequently, enhanced energy density and service life. Virtually, all recent research concerning Mg anodes paid more attention to the corrosion rate of Mg anodes at OCP, which is normally considered as the evaluation criterion of wasteful-discharge rate under varied applied current. However, recent work of Deng et al. [29] indicates that the wasteful anode discharge of Mg electrode is greatly dependent on the applied current density. To assess the wasteful anode discharge behavior of Mg in time of discharging by the corrosion rate measured at OCP is not advisable. Different Mg alloys show varied increasing rate of

real-time wasteful-discharge rate with the rising applied current density, resulting from different extent of NDE. Therefore, advanced Mg anodes should have low wasteful-discharge rate during discharging at different current densities (inhibited NDE) rather than low corrosion rate simply at OCP condition.

Our previous research indicates that binary Mg-Ca alloys possess great potential as environmentally benign anode materials with superior discharge properties [30, 31]. Micro-alloyed Mg -0.1 wt.%Ca alloy shows higher discharge voltage and energy density than that of high purity Mg, AM50 and AZ31 alloys measured in a lab-made Mg-air full cell. Nevertheless, the voltage (e.g., 1.6 V at 0.5 mA cm^{-2}) and peak energy density (1800 Wh kg^{-1}) should be improved towards the theoretical value, which is 3.1 V and 6.8 kWh kg^{-1} respectively. Thus, further improvement on Mg-Ca based anodes is desirable via micro alloying with other elements. Indium (In) as an alloying element has been successfully used in Al anodes for primary Al batteries to improve relevant discharge performance [32-36]. The In-induced activation on Al anodes is proposed to be the result of film disruption by In re-deposition back to anode surface. Likewise, recently, some work has been done to investigate the effect of In addition on performance of some Mg anodes [22, 26, 37-39]. Improvement to different extent has been achieved. As reported, the discharge voltage at 10 mA cm^{-2} of a Mg-air cell increases from 1.16 V to 1.22 V after replacing the Mg -9 wt.%Al anode with Mg -9 wt.%Al -1 wt.%In [39]. Interestingly, almost all the relevant work regarding In-alloyed Mg anodes is based on Mg-Al alloys with high Al contents, from 3 - 9 wt.%. Mg-Al based anodes normally output low discharge voltage because of low open circuit voltage (OCV) and relatively protective surface oxidation film caused by accumulation of Al_2O_3 [40-42]. In such cases, all the studied Mg anodes retain a low cell voltage (around 1.2 V at 10 mA cm^{-2}) although an enhancement by In addition (popularly 1 wt.%) is achieved. On the other side, the corrosion rate of Mg anodes in NaCl-based electrolytes at OCP is accelerated after In alloying. Nevertheless, no information regarding the wasteful-discharge of these Mg-In anodes during discharge can be found. The possible different dissolution behavior at OCP condition and with applied current is neglected. Of late, Gore et al. [43] investigated the effect of In^{3+} ions existing in the electrolyte on the dissolution kinetics of Mg at OCP as well as under polarization. The dissolution rate of a high purity Mg at OCP is increased after addition of 1 mM $InCl_3$ into 0.1 M NaCl solution, whilst the self-corrosion under applied current densities is inhibited in the solution with $InCl_3$. Although the inhibition mechanism of In remains

unclear, the authors propose that $InCl_3$ as a electrolyte additive could be an effective approach for developing Mg primary batteries with high performance. However, it should be noted that free In^{3+} ions would be consumed via precipitation as oxide or hydroxide during long-term battery operation, which consequently negatively affects the battery properties. A better alternative could be alloying Mg anode with an appropriate In content. In such a case, In ions are constantly replenished along with the continuous dissolution of anode materials.

Considering all the aforementioned strategies concerning Mg anodes development, we suppose that Mg micro alloyed with Ca and In is a high quality anode of aqueous Mg-air batteries. In the present work, two micro-alloyed Mg-Ca-In alloys are fabricated and appraised as anodes in half-cell and a lab-made Mg-air full cell. Corrosion rates at OCP condition and wasteful-discharge rates under different current densities are measured and compared. The activation effect of In on Mg anodes is confirmed and the activation mechanism is investigated from different aspects.

2. EXPERIMENTAL SECTION

2.1 Materials preparation

Conventional gravity casting method was utilized to prepare all the micro-alloyed Mg anodes with nominal composition of Mg -0.1%Ca, Mg -0.1%Ca -0.2%In and Mg -0.2%Ca -0.4%In (hereafter weight percent). The raw materials used for alloy preparation were pure Mg ingot (MAGONTEC Ltd., Australia), Ca chips (Alfa Aesar GmbH & Co. KG, Germany) and In bars (Grirem Advanced Materials Co., Ltd., China) with purity of 99.96 wt.%, 99.9 wt.% and 99.95 wt.% respectively. All the raw materials for each alloy were melted at 760 ℃ in a steel crucible coated with boron nitride under protection of Ar/SF_6 (5:1) mixed gas to prevent melt oxidation and burning. Afterwards, the melts were cast and then quenched in water with a cylindrical steel mold with diameter of 60 mm preheated to 300 ℃. The actual chemical compositions of all processed materials were shown in Table 1 as analyzed by spark spectrometer (spark OES, Ametek-Spectro) and X-ray micro fluorescence (μXRF, Bruker). The impurities Fe, Ni and Cu [12, 44-47] that have deleterious influence on Mg corrosion resistance were below the generally accepted tolerance limits.

Table 1. Chemical composition of as-cast Mg anodes (wt.%).

Materials	Ca	In	Fe	Ni	Cu	Al	Mn	Si	Mg
Mg-0.1Ca	0.07	-	0.0018	0.0011	0.0012	< 0.01	0.017	0.0036	Bal.
Mg-0.1Ca-0.2In	0.09	0.25	0.0016	0.0008	0.0009	< 0.01	0.014	0.0052	Bal.
Mg-0.2Ca-0.4In	0.19	0.37	0.0043	0.0008	0.0009	< 0.01	0.015	0.0052	Bal.

2.2 Microstructure characterization

All specimens after embedding in resin were carefully ground and polished to obtain high-quality surface for microstructure observation. Grinding process was carried out on silicon carbide papers consecutively up to 4000 grit. Afterwards, samples were polished to remove scratches using a water-free oxide polishing suspension (OPS) containing SiO_2 followed by a cleaning process in ethanol by ultrasonication. Second phase morphology and distribution were observed with a scanning electron microscope (SEM, TESCAN VEGA3) combined with energy dispersive X-ray spectroscopy (EDS) to analyze the phase composition. Elemental mapping was also obtained with the SEM to investigate the distribution of each selected alloying element via backscattered-electrons (BSE) detector at 15kV. Besides, atomic Force Microscopy (AFM, Nanowizard, JPK Instruments AG) combined with Scanning Kelvin Probe force microscopy (SKPFM) was utilized to measure the Volta potential difference between second phase particles and the Mg matrix. The adopted silicon probe supplied by Innovative Solutions Bulgaria Ltd. (Bulgaria) is coated with a Cr/Pt conductive coating and possesses a resonance frequency of 75 kHz and a force constant of 3 N m^{-1}. The measurements were conducted immediately after sample polishing via the aforementioned processes.

2.3 Corrosion and wasteful anode discharge rate determination

The corrosion rates of all prepared alloys at OCP and wasteful-discharge rates during discharge were determined by the commonly accepted hydrogen evolution (HE) method at 23 ± 2 ℃. Hydrogen gas produced during immersion at OCP was collected simultaneously via a widely used set-up combining a funnel and an inverted burette [48, 49]. The solution used throughout was 3.5 wt.% NaCl solution based on deionized water. The volume of solution was 350 ml for each test. Two bulk specimens with a total surface area of approximately 14 cm^2 were used for each measurement applied with stirring by

an electromagnetic stirrer at 350 rpm. HE rates during discharge were measured with the same set-up adopted in our recent work [29]. Each sample was embedded in epoxy exposing a working surface of 15× 15 mm. A potentiostat (Gamry interface 1000) was used to apply specific current densities with a classic three-electrode system consisting of a Pt wire counter electrode, a saturated-KCl filled Ag/AgCl reference electrode and an Mg electrode. HE rates of each Mg anode were determined when discharge at varied current densities, i.e. 1, 5, 10 and 20 mA cm^{-2} for 8 h, 2 h, 2 h and 1 h, respectively. Each measurement was conducted for three times to ensure data reproducibility.

2.4 Electrochemical measurements

The aforementioned three-electrode system was also applied to measure the potentiodynamic polarization curves and electrochemical impedance spectra (EIS) via a Gamry Interface-1000 potentiostat. Samples with 1 cm^2 working surface area were utilized. Anodic and cathodic polarization curves were measured separately with a scanning rate of 1 mV s^{-1} after a stabilization period of one hour in the solution to obtain a relatively stable OCP. The scanning potential of anodic curves was – 10 mV versus OCP upwards to – 1.4 V versus the reference electrode, while for cathodic curves it was + 10 mV versus OCP downwards to – 2.2 V versus the reference. Besides, polarization curves were also obtained after immersion in the solution for 48 h via direct scanning from – 250 mV to + 400 mV versus OCP. For each alloy, the EIS was determined after immersion for different period, i.e., 0.5, 4, 8, 24, and 48 h, to evaluate the corrosion evolution. The scanned frequency range was 100 kHz to 0.01 Hz, and the sinusoidal AC voltage was 10 mV rms. The EIS results were fitted by Zview software according to a proposed equivalent circuit. All the electrochemical measurements were carried out for three times with diverse specimens to ensure data reproducibility.

Half-cell discharge curves were recorded via the Gamry potentiostat with the aforementioned three-electrode system at constant current densities. The surface area of each specimen as working electrode was 1 cm^2. EIS was also determined after discharge, such as at 1 mA cm^{-2} for 8 h and 20 mA cm^{-2} for 2 h, to evaluate the discharge activity of each Mg anode. The lowest scanning frequency was set as 0.1 Hz for the EIS measurement after discharge. Besides, the surface and cross-sectional morphologies after discharge were observed under SEM. X-ray photoelectron spectroscopic (XPS) measurements for

investigating the anode surface after discharge were performed using a Kratos Axis Ultra DLD instrument (Kratos Analytical, Manchester UK) equipped with a monochromatic Al Kα anode working at 15 kV (225 W). The pass energy for recording of the survey spectra and region spectra was 160 eV and 20 eV, respectively. The investigated area of the sample was selected as 700×300μm. In order to analyze the inside of the surface film, Ar etching was applied for 30 min by a rate of 10 nm min^{-1} with respect to Ta_2O_5. The acceleration voltage and extraction current for the Ar etching were 3.8 kV and 160 mA. The XPS data were validated and evaluated using CASA-XPS software (version 2.3.18). Background subtraction (U2 Tougaard) was conducted for calculation and deconvolution of the region spectrum. The C 1s signal was used for spectra calibration and adjusted to 284.5 eV.

2.5 Mg-air battery tests

Discharge properties of prepared Mg anodes were evaluated in a lab-made Mg-air full cell. The adopted cathode, with surface area of around 2.5 cm^2, was a commercial air cathode (Gaskatel GmbH, No. 82011) with C/MnO_2 catalysts, nickel mesh current-collector and PTFE gas diffusion layer, while the electrolyte was 3.5 wt.% NaCl solution. The anode was an alloy specimen embedded in resin with exposing surface area of approximately 2.2 cm^2. An as-cast AZ31 Mg alloy, which is commercially accepted as anode materials for Mg batteries, was tested as well for comparison. Cell voltage was recorded simultaneously during discharge at different current densities for 1 h. Afterwards, the average voltage and power density at different current densities were calculated.

Battery discharge tests were performed in a constructed Mg-air full cell with the schematic shown in Fig. 1 to evaluate the service life of varied anodes. The anode was strip-shaped sample corresponding to each Mg alloy. The dimension of the anode working part immersed into the electrolyte is 30×5×2.5 mm. The Mg-air cell assembled with varied anode material was discharged at constant current of 23.75 and 47.5 mA, which respectively correspond to an initial current density of 5 and 10 mA cm^{-2}. A cut-off voltage of 0.5 V was set for each test. Afterwards, service life and average voltage of the Mg-air cell with different anode can be obtained from the voltage-time curves. Besides, anodic efficiency, discharge capacity and energy density can be calculated via the same equations used in other literatures [30, 31], as the weight of consumed anode was known. This kind of battery discharge test for all anodes

at different current densities were repeated twice. Good reproducibility was indicated as slight deviation (below 5%) between the two measurements was obtained.

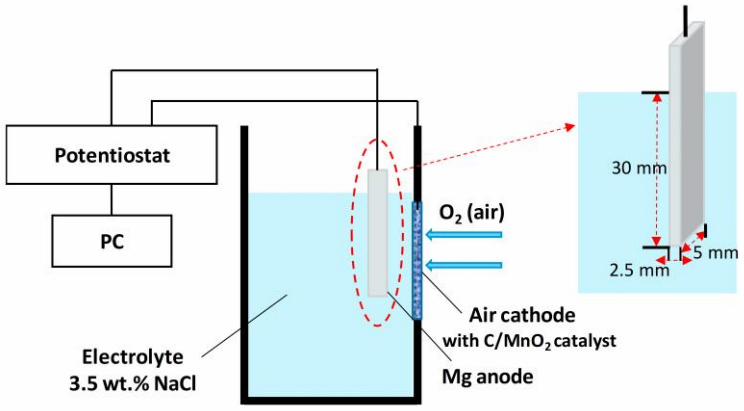

Fig. 1. Schematic of a lab-made Mg-air cell for battery discharge test.

3. RESULTS AND DISCUSSION

3.1 Microstructure

Fig. 2(a-c) presents the SEM images of all prepared Mg alloys, indicating increasing amount of intermetallic particles (IMPs) with the rising In content. The IMPs in Mg-0.1Ca alloy are mainly MgCaSi because of the existence of trace Si in the alloy. This is consistent with the solidification simulation results reported by Jin et al. [50], which indicates that MgCaSi phase solidifies prior to Mg_2Ca in the Mg -0.5 wt.%Zn -0.2 wt.%Ca system with 145 ppm Si. The chemical compositions of the IMPs are also analyzed by EDS (one representative result is indicated in Table 2), proving the preferential formation of MgCaSi. In the case of Mg-Ca-In alloys, two types of IMPs, i.e. Mg-Ca-Si and Mg-Ca-In-Si, are determined by EDS and elemental mapping as presented in Fig. 2(d-g) and Table 2. The stoichiometry of Mg-Ca-In-Si phases is not known since there is a paucity of phase diagram or relevant thermodynamic data available for predicting the equilibrium phases in Mg-Ca-In based alloys, e.g. using Pandat™ 2017. Some literatures reported Mg-Ca-In precipitates with a Ca/In content ratio of 2:1 after aging heat treatment [51, 52], but Si was not included in these work. Apparently, no fixed ratio of Ca/In is detected in the present work from the EDX results and Si indicates a highly random content in the Mg-Ca-In-Si IMPs. Nevertheless, determination of the specific stoichiometry and crystal structure of Si-enriched Mg-Ca-In phases are beyond the scope of this work. Much attention is paid to

the electrochemical potential of these IMPs relative to Mg matrix, which is more relevant to the self-corrosion and discharge performance of Mg anodes. Fig. 2(h-j) presents the Volta potential map and corresponding Volta potential along line *I* and *II* in Mg-0.1Ca-0.2In alloy obtained by SKPFM. The results indicate that all the IMPs have higher Volta potential than surrounding Mg matrix. Micro galvanic couples, in which the matrix acts as anode and IMP acts as cathode, are pronounced during corrosion and discharge process. Thus, preferential dissolution of Mg matrix is favored by the existence of different IMPs.

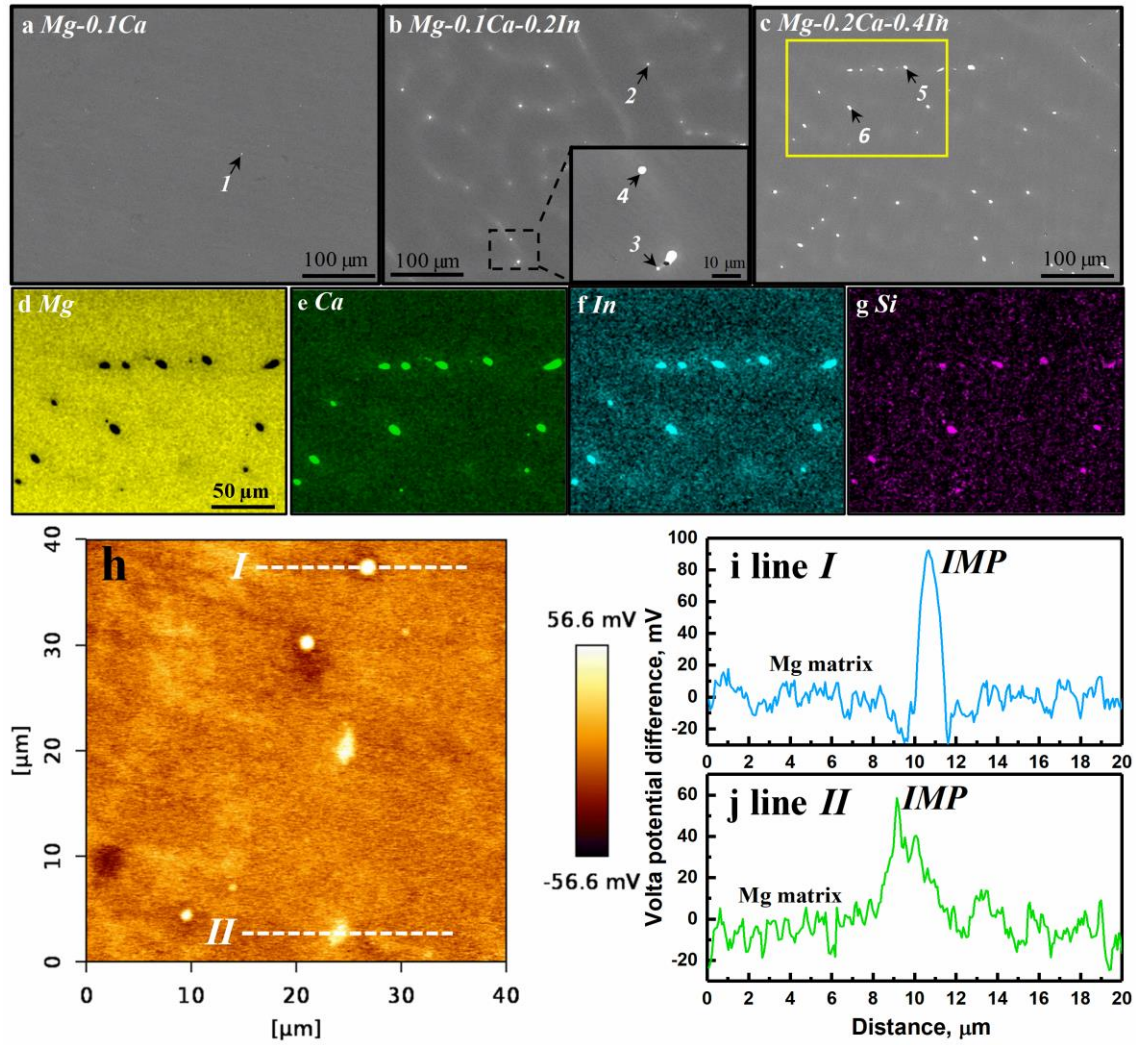

Fig. 2. (a-c) SEM images of three as-cast Mg alloys; (d-g) Corresponding elemental mappings for the marked region in (c) Mg-0.2Ca-0.4In alloy. (h) Volta potential map of Mg-0.1Ca-0.2In alloy obtained by SKPFM. (i, j) Corresponding Volta potential along line *I* and *II*, respectively.

Table 2. Chemical compositions of the particles marked in Figure 2(a-c) by EDS analysis (wt.%).

Particle	*1*	*2*	*3*	*4*	*5*	*6*
Mg	73.5	57.9	65.9	84.0	75.7	65.3
Ca	13.9	24.6	20.4	8.4	18.7	25.0
In	/	9.3	/	7.3	5.2	6.3
Si	12.6	8.2	13.7	0.3	0.4	3.4

3.2 Half-cell discharge properties

Discharge potential at different current densities was measured in half-cell and presented in Fig. 3 (a-d). Obviously, more negative potential is achieved by In addition to Mg-0.1Ca anode, which would consequently contribute to higher output voltage of Mg-air full cell. It is noticeable that both Mg-Ca-In anodes exhibit a negatively shifting potential at the beginning stage before presenting a relatively stable potential afterwards. The time for reaching the steady discharge differs with varied current densities，such as approximately 3 h at 5 mA cm^{-2} while less than 1 h at 20 mA cm^{-2}. Besides, at all applied current densities, Mg-0.2Ca-0.4In anode requires less time for the stabilization than Mg-0.1Ca-0.2In. The activation of Mg anodes induced by In addition is probably related to the re-deposition of In onto the anode surface from In^{3+} produced by anode dissolution as proposed by Li et al. [22]. A displacement reaction contributing to the re-precipitation of In is described in Eq. 1 as assumed by Gore et al. [43].

$$3Mg\ (s) + 2In^{3+}\ (aq) = 3Mg^{2+}\ (aq) + 2In\ (s) \quad (1)$$

XPS measurements were applied in attempt to prove the existence of metallic In either for the surface of a Mg-Al-Zn-In anode after discharge in blank 3.5 wt.% NaCl solution [22] or a pure Mg surface after immersion in 0.1 M NaCl + 1 mM $InCl_3$ solution [43]. However, from the exhibited results, the existence of In_2O_3/$In(OH)_3$ is more pronounced than pure In. Dissimilarly, in this work, apart from the surface outermost layer, the inside of the surface film on Mg-0.2Ca-0.4In anode after discharge is also analyzed by XPS after Ar etching for 30 min by a rate of 10 nm min^{-1}. The survey spectrum related to the inside film presented in Fig. 4a indicates the presence of Na, Cl and O, ensuring that the

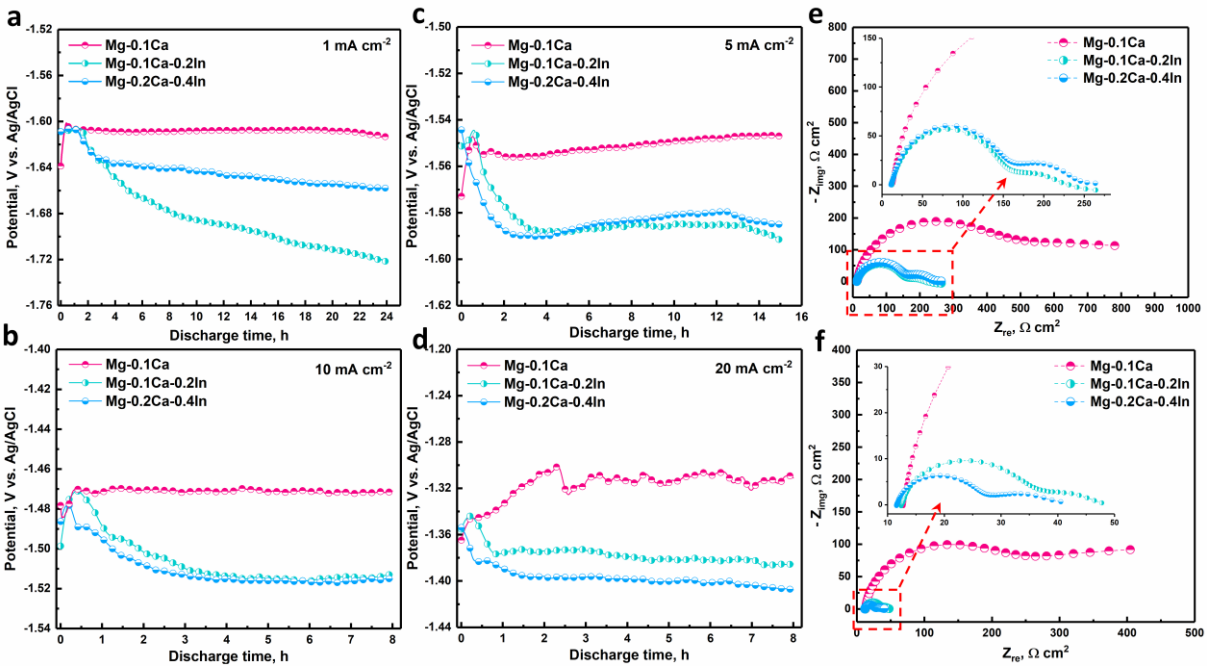

Fig. 3. (a-d) Half-cell discharge curves of as-cast Mg anodes at different current densities in 3.5 wt.% NaCl solution. (e, f) Nyquist plots of EIS measured after discharge at 1 mA cm^{-2} for 8 h and 20 mA cm^{-2} for 2 h, respectively.

measurement is performed still on the products film rather than anode substrate. The In 3d XPS region spectrum indicated in Fig. 4b confirms the existence of metallic In. The In 3d 5/2 peak at 443.55 eV and In 3d 3/2 peak at 451.09 eV, with a specific distance of 7.54 eV, are related to indium in the form of elementary In [53, 54]. It is noteworthy that no information of metallic Ca is found from the XPS spectra. Therefore, the possibility can be excluded that In signal in XPS results may be from the possible existence of IMPs in discharge products layer, since Ca shows a much higher content than In in the mentioned IMPs as shown by EDS (Table 2). Note that, however, metallic In has not been detected by the XPS performed on the surface outermost layer without etching, implying that In re-deposition takes place at the vicinity of anode substrate. Since In has more positive electrochemical potential than Mg, the re-deposition of metallic In on Mg anode substrate would definitely promote the dissolution of Mg driven by micro galvanic couples and, consequently, increase the discharge activity. Meanwhile, the redeposited In would be detached from the anode substrate after dissolution of surrounding Mg matrix. It is convincible that the re-deposition and detachment of In could reach a dynamic equilibrium after a period, leading to relatively stable discharge voltage. Because of the low In contents in the anodes (0.2

and 0.4 wt.%) studied in this work, several hours are needed before reaching the dynamic equilibrium as indicated from the discharge curves due to insufficient In^{3+} ions within initial discharge period. Reasonably, enhanced discharge current density and higher In content in anode, which both contribute to a higher concentration of generated In^{3+}, are able to decrease the time required for the stabilization process. Similar phenomenon is not found from other published work regarding Mg anodes with In [22, 37, 39, 55], possibly because of the relatively higher applied In content (e.g., 1 wt.%) and the synergetic effect of other elements in high contents.

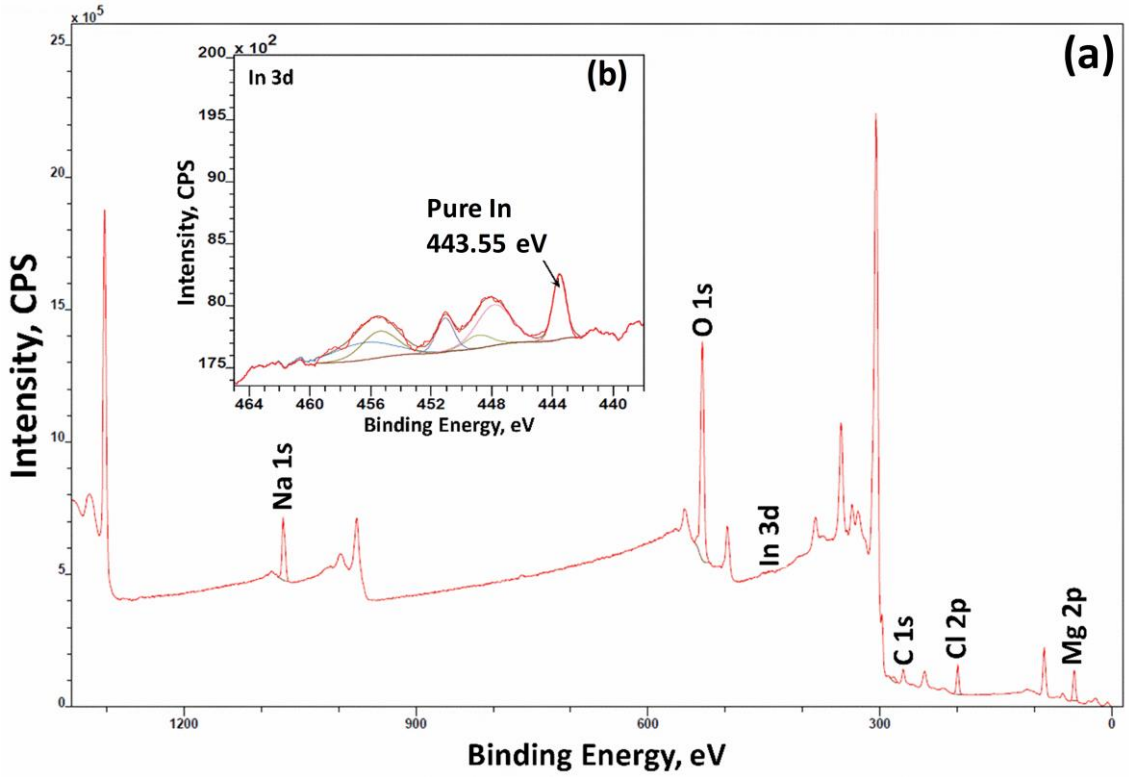

Fig. 4. (a) XPS survey spectrum and (b) High resolution In 3d region spectrum obtained on the Mg-0.2Ca-0.4In anode surface after discharge at 1 mA cm^{-2} for one hour in 3.5 wt.% NaCl solution (after Ar etching for 30 min by a rate of 10 nm min^{-1}).

Moreover, it is noteworthy that the discharge potential of Mg-0.2Ca-0.4In anode is more positive than Mg-0.1Ca-0.2In at 1 mA cm^{-2}, but shows a tendency of being comparable or more negative with the increased current density. EIS determined after discharge are presented in Fig. 3e and f, illustrating varying discharge activity under different current densities. Remarkably, In-based Mg-Ca anodes show significantly lower electrochemical impedance after discharge than binary Mg-0.1Ca, corresponding to

enhanced discharge activity and decreased overpotential by In addition. Mg-0.2Ca-0.4In shows slightly higher electrochemical impedance than Mg-0.1Ca-0.2In measured after discharge at 1 mA cm^{-2}, while lower regarding 20 mA cm^{-2}. Therefore, it is speculated that different In content would lead to varying discharge activity of the Mg-Ca-In anodes with relevance to varied discharge current densities. Besides, the surface morphologies after discharge presented in Fig. 5 (a-c) explicate altered diffusion overpotential during discharge process after In addition. Mg-0.1Ca anode surface is densely and integrally covered by discharge products (Fig. 5a), which causes large transport overpotential. In contrast, the discharge products film on the surface of Mg-Ca-In anodes is deformed (Fig. 5b and c). Dense discharge products are only found at specific spots. Most areas are covered by thin and porous products film. Besides, some cavities without discharge products are apparently visible from the Mg-Ca-In surface after discharge, indicating effortless breakage and peeling of the products. Consequently, the transport overpotential during discharge decreases, being conducive to achieve enhanced battery voltage. The exfoliation of products is promoted by In addition possibly because of the accumulation of redeposited In on the interface of anode substrate and products film, which certainly reduces the adherence between the substrate and products, similar to the proposed activation mechanism of In on Al anodes [33].

In addition, the cross-sectional morphologies after discharge are illustrated in Fig. 5 (d-f) to evaluate the possible occurrence of "chunk effect", which has been proved to have significant influence on the anodic efficiency and capacity of Mg anodes during discharge. No detached metallic pieces can be found from the cross sections of Mg-0.1Ca and Mg-0.1Ca-0.2In anodes, implying that no large loss of anodic efficiency would be caused by chunk effect. On the contrary, large metallic pieces, which are undissolved Mg matrix as confirmed by EDS (not shown here), are detached from the substrate and exist in the discharge products layer. The loss of these portions would certainly result in large efficiency loss of Mg-0.2Ca-0.4In anode and, thus, reduce the energy density of Mg-air cell. The chunk effect is related to the non-uniform dissolution of Mg-0.2Ca-0.4In anode, which is possibly due to the higher amount of IMPs and inhomogeneous deposition of In.

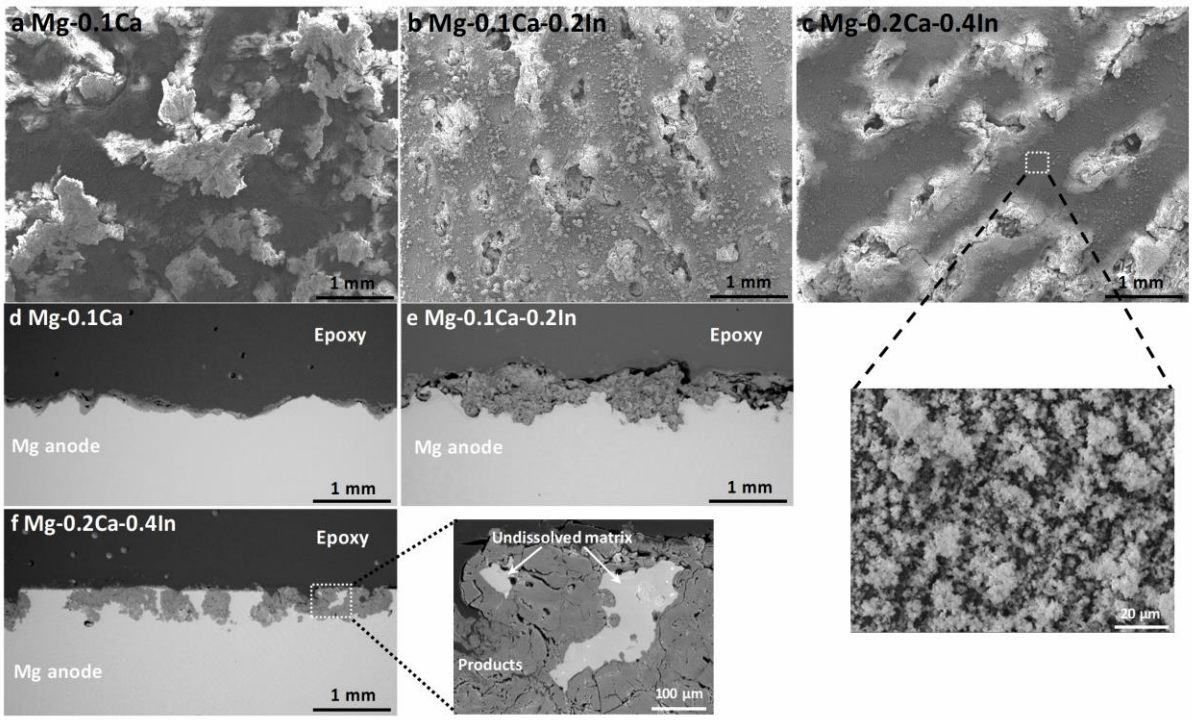

Fig. 5. Surface morphology after discharge at 5 mA cm^{-2} for 15 h in 3.5 wt.% NaCl solution corresponds to (a) Mg-0.1Ca, (b) Mg-0.1Ca-0.2In and (c) Mg-0.2Ca-0.4In. Cross-sectional morphology of (e) Mg-0.1Ca, (d) Mg-0.1Ca-0.2In and (f) Mg-0.2Ca-0.4In after discharge at 5 mA cm^{-2} for 15 h.

3.3 Corrosion and wasteful anode discharge rate

Importantly, Mg anodes should have low corrosion rate during non-discharge interval (at OCP condition) to ensure relatively long battery life. The corrosion rate of the micro-alloyed anode are evaluated via HE tests as indicated in Fig. 6a. Generally, the HE rate (V_H) of Mg-0.1Ca anode is enhanced with addition of In, but the acceleration is slight at 0.2 wt.% In load. The corrosion rate (P_H), which can be calculated via the formula $P_H = 2.088\ V_H$ [56], is 0.44 mm y^{-1} for Mg-0.1Ca and 0.48 mm y^{-1} for Mg-0.1Ca-0.2In, lower than that of majority of Mg alloys in NaCl solution with similar concentration as summed up in literatures [57, 58]. Before reaching the stage with steady corrosion related to the formation of a protective film, all the studied alloys show a relatively fast corrosion rate at the initial stage indicated by the hydrogen evolution curves. Interestingly, Mg-0.1Ca shows slightly higher corrosion rate than Mg-0.1Ca-0.2In alloy during the first several hours, differing from the situation in the latter period. EIS results presented in Fig. 6 (c-f) reveal the same variation of the corrosion rate corresponding to all the studied Mg alloys during the whole immersion period. R_{sum},

which equals to the sum of charge transfer resistance (R_{ct}) and film resistance (R_f), is used to evaluate the corrosion resistance of Mg alloys. R_{ct} and R_f can be obtained via fitting the EIS results according to the proposed equivalent circuit as shown in Fig. S1 [59]. Apparently, from Figure 6c, R_{sum} of Mg-0.1Ca is slightly lower than that of Mg-0.1Ca-0.2In during the initial immersion period of 8 h, indicating higher corrosion rate in this period. With prolonging immersion time, R_{sum} of Mg-0.1Ca increases and tends to be higher than Mg-0.1Ca-0.2In, corresponding to the lowering corrosion rate as shown by HE tests. According to the polarization curves after one-hour OCP measurement (Fig. 6h), the cathodic reaction kinetics is weakened after addition of 0.2 wt.% In to Mg-0.1Ca, whilst no significant variation is indicated regarding anodic reaction kinetics. However, after immersion for 48 h, Mg-0.1Ca shows

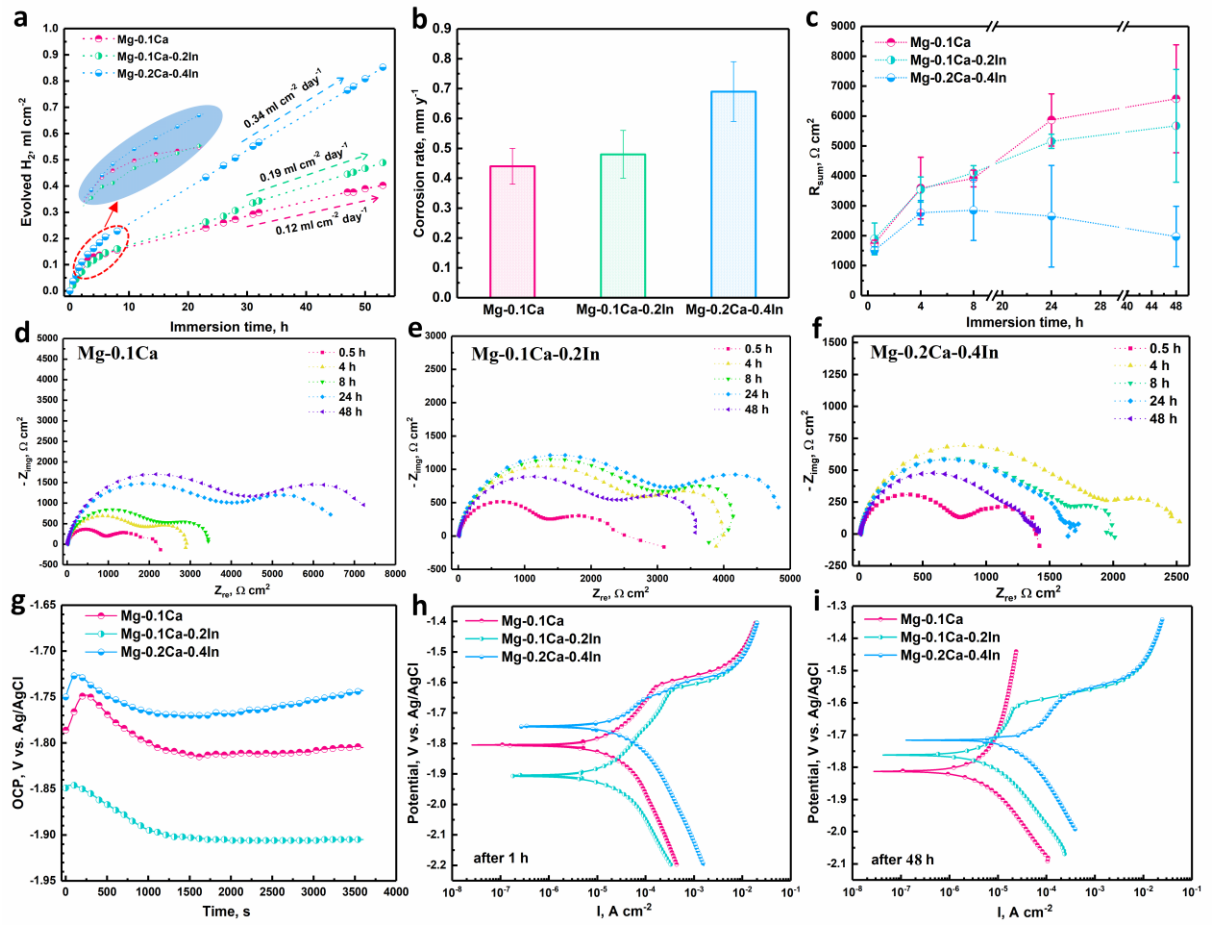

Fig. 6. (a) Hydrogen evolution of as-cast alloys during immersion. (b) Calculated average corrosion rate during immersion of 52 h based on hydrogen evolution. (c) Sum of charge transfer resistance and film resistance varies with immersion time obtained via EIS fitting results. (d-f) Nyquist plots from EIS of as-cast alloys after immersion for different time. (g) OCP of as-cast Mg anodes. (h, i) Polarization curves after immersion for 1 h and 48 h, respectively, without IR compensation. Note that all the measurements are carried out in 3.5 wt.% NaCl solution.

moderated kinetics for both anodic and cathodic reactions compared to Mg-0.1Ca-0.2In (Fig. 6i). A protective film forms on the surface of Mg-0.1Ca after long time immersion, speculated from the anodic polarization curve that shows dilatorily increasing current density within the scanning potential range. In contrast, a breakdown potential, after which the current density increases rapidly, can be found with respect to the Mg-Ca-In alloys. According to the EIS results presented in Fig. 6(d-f), the film resistance of Mg-0.1Ca increases from 800 Ω cm^2 at the beginning to 4000 Ω cm^2 after 48 h. By contrast, the film resistance alteration of Mg-0.1Ca-0.2In is slight, from 1200 to 2000 Ω cm^2. The much higher film resistance also indicates a more protective film formed on Mg-0.1Ca surface after long time immersion. The absence of a film with sufficient protection, which is because of the accumulation of redeposited In close to Mg substrate as mentioned above, is one of the reason for the increased corrosion rate at OCP. Another reason should be the additional galvanic corrosion caused by the contact of Mg substrate and re-precipitated metallic In. Noticeably, Mg-0.2Ca-0.4In shows higher corrosion rate than other two alloys during the whole immersion period. The slightly faster corrosion at the beginning is due to the enhanced cathodic reaction kinetics caused by more cathodic IMPs as the result of higher alloying content. Afterwards, the much higher corrosion rate compared with other alloys is because of more re-deposition of In due to the higher In content, which favors a higher concentration of In^{3+} ion.

Service life and energy density of Mg-air batteries are tightly dependent on the wasteful-discharge rate of anodes in time of operating, which is the main issue hindering their application. It must be noted that corrosion rate measured under OCP condition is unable to exactly reflect the wasteful-discharge rate during discharge at different current densities as mentioned above [29]. Therefore, the wasteful-discharge behavior of the prepared Mg anodes were also determined via HE tests with varied applied current density as depicted in Fig. 7 (a-d). Hydrogen evolution rate at varying current densities (Fig. 7e) are calculated according to the steady-state HE and then the wasteful-discharge rate (converted to current density) (Fig. 7f) are obtained accordingly using Faraday's law. Apparently known from the presented results, all the studied anodes exhibit a linearly increasing wasteful-discharge rate as a function of applied current density over the whole current density range, which is consistent with the well-known NDE on Mg metal. The data are linearly fitted into straight lines with different slopes, *k*, which reflects the increasing rate of wasteful-discharge rate with raising applied current density. The

slope is 0.68, 0.29 and 0.39 for Mg-0.1Ca, Mg-0.1Ca-0.2In and Mg-0.2Ca-0.4In, respectively. Hence, the wasteful-discharge rate of Mg-0.1Ca-0.2In is similar to that of Mg-0.1Ca at 1 mA cm^{-2} current density, but shows a tendency of being much lower than Mg-0.1Ca with increasing current density. So is the Mg-0.2Ca-0.4In anode, although the slope is larger than Mg-0.1Ca-0.2In. The different slopes demonstrate varied extent of NDE happening on the three Mg anodes. In general, the addition of In suppresses the NDE and reduces the wasteful-discharge rate of Mg-Ca anode, which is definitely beneficial for achieving higher anodic efficiency. Additionally, the Mg-Ca-In alloys show significantly lower wasteful-discharge rate and *k* than high purity Mg, AZ31 and AM50 alloys (see Fig. S2), which are widely used as anode materials. No doubt, this issue is related with NDE. However, unfortunately, the mechanism of NDE is still a controversial puzzle despite several models has been proposed in last decades in attempt to explain it [12, 13, 60-63]. Therefore, the reason for the inhibited NDE by In addition deserves more effort, but is not within the scope of this work.

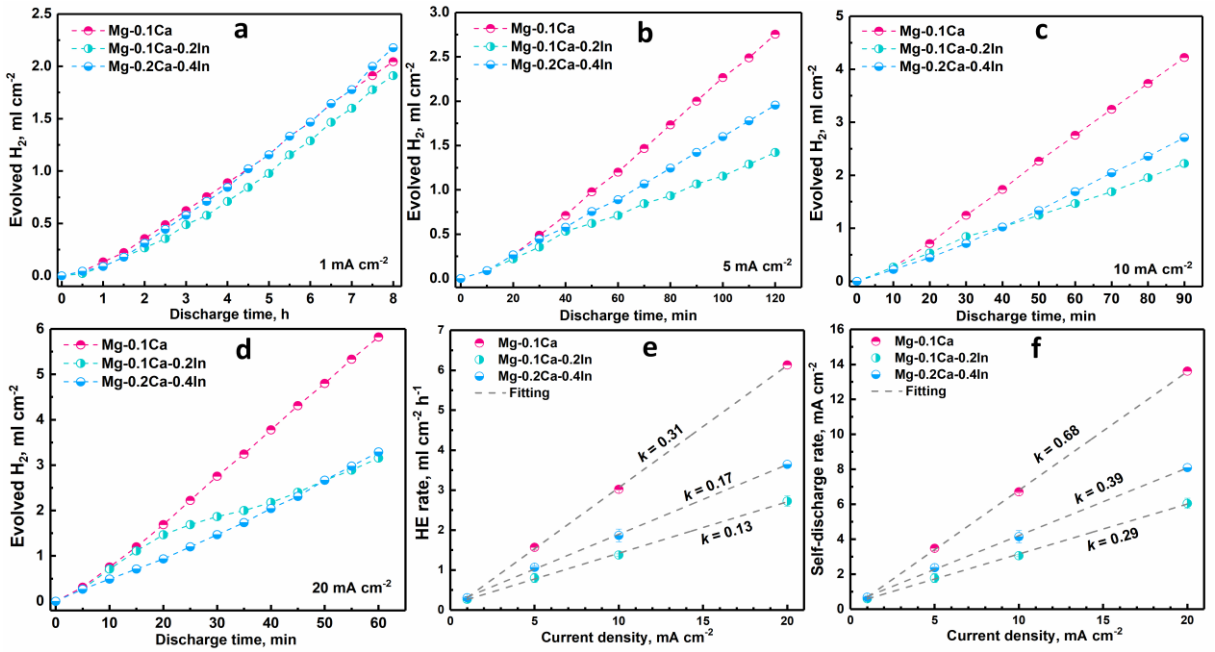

Fig. 7. (a-d) Hydrogen evolution of as-cast Mg anodes during discharge at different current densities in 3.5 wt.% NaCl solution. Typical results of triplicate measurements are shown. (e) Hydrogen evolution rate as a function of discharge current density. (f) Wasteful-discharge rate associated with HE as a function of discharge current density. Linearly fitting results are presented in (e, f) with a slope k. Hydrogen evolution rate is determined based on the steady-state HE. Error bar is not visible when the standard deviation is less than the symbol.

3.4 Mg-air battery tests

Fig. 8a illustrates the cell voltage and power density of a lab-made Mg-air battery adopting different Mg anodes. Note, it is not sensible to compare the voltage-involved battery properties between different literature sources as varied cathode materials are used, which is also one important limiting factor for battery voltage. Therefore, in this work, AZ31 is included for comparison, as it is a commercially acceptable anode material for aqueous Mg primary batteries. Obviously, the Mg-air system based on Mg-0.1Ca shows much higher cell voltage than that based on AZ31, which is consistent with the previously reported results [30]. Besides, the cell voltage is further enhanced by replacing the Mg-0.1Ca anode with Mg-Ca-In anodes, especially at high current densities. For instance, at 5 mA cm^{-2}, the voltage is 1.31, 1.40 and 1.46 V for the battery with AZ31, Mg-0.1Ca and Mg-0.1Ca-0.2In anode, separately, while 0.68, 0.78 and 0.92 V respectively at 40 mA cm^{-2}. In addition, the peak power density is enhanced as well by the adoption of In-based anodes. The battery with Mg-0.1Ca-0.2In anode possesses a peak power density of 39.8 mW cm^{-2} at 55 mA cm^{-2}, while the batteries with AZ31 and Mg-0.1Ca anode show peak power densities of 27.8 and 31.2 mW cm^{-2} individually. Fig. S3 presents the results of intermittent discharge testing to evaluate the re-operation property with regard to the battery with different anodes. Apparently, the battery with Mg-Ca anode shows low voltage at the very beginning of the re-operation session after a non-discharge interval due to large overpotential caused by surface film. By comparison, the battery with Mg-Ca-In anode is able to be reactivated immediately during re-operation attributed to the less compact film and In re-deposition.

The voltage profiles for battery discharge tests with the configuration presented in Fig. 1 are depicted in Fig. 8b and c, and the relevant battery properties obtained are listed in Table 3. Not surprisingly, the batteries based on Mg-Ca-In anodes exhibit higher voltage than those based on AZ31 and binary Mg-0.1Ca anode. Importantly, battery service life is significantly enhanced via utilizing Mg-Ca-In anodes. Under 23.75 mA constant current load, the service life is 39.2, 40.6, 49.1 and 44.4 h for the cell with AZ31, Mg-0.1Ca, Mg-0.1Ca-0.2In and Mg-0.2Ca-0.4In anodes, independently. The improvement of battery service life associated with In addition is mainly due to the increased anodic efficiency of the anode material as indicated in Table 3. With 0.2 wt.% In addition, the anodic efficiency of Mg-0.1Ca

anode is boosted from 66.4% to 80.2% at 23.75 mA and from 61.9% to 77.8% at 47.5 mA. The improvement on anodic efficiency is attributed to the inhibited wasteful-discharge rate by the addition of In and the absence of chunk effect as mentioned in above sections. Moreover, attributing to the improved cell voltage and anodic efficiency, the energy density of the tested Mg-air battery is enhanced consequently. The system with Mg-0.1Ca-0.2In anode shows an energy density of 2259 Wh kg^{-1} at 23.75 mA. For comparison, 1629 and 1835 Wh kg^{-1} for the cell with AZ31 and Mg-0.1Ca anodes are obtained, respectively. In other words, an enhancement of 39% can be achieved via replacing AZ31 by Mg-0.1Ca-0.2In as the anode.

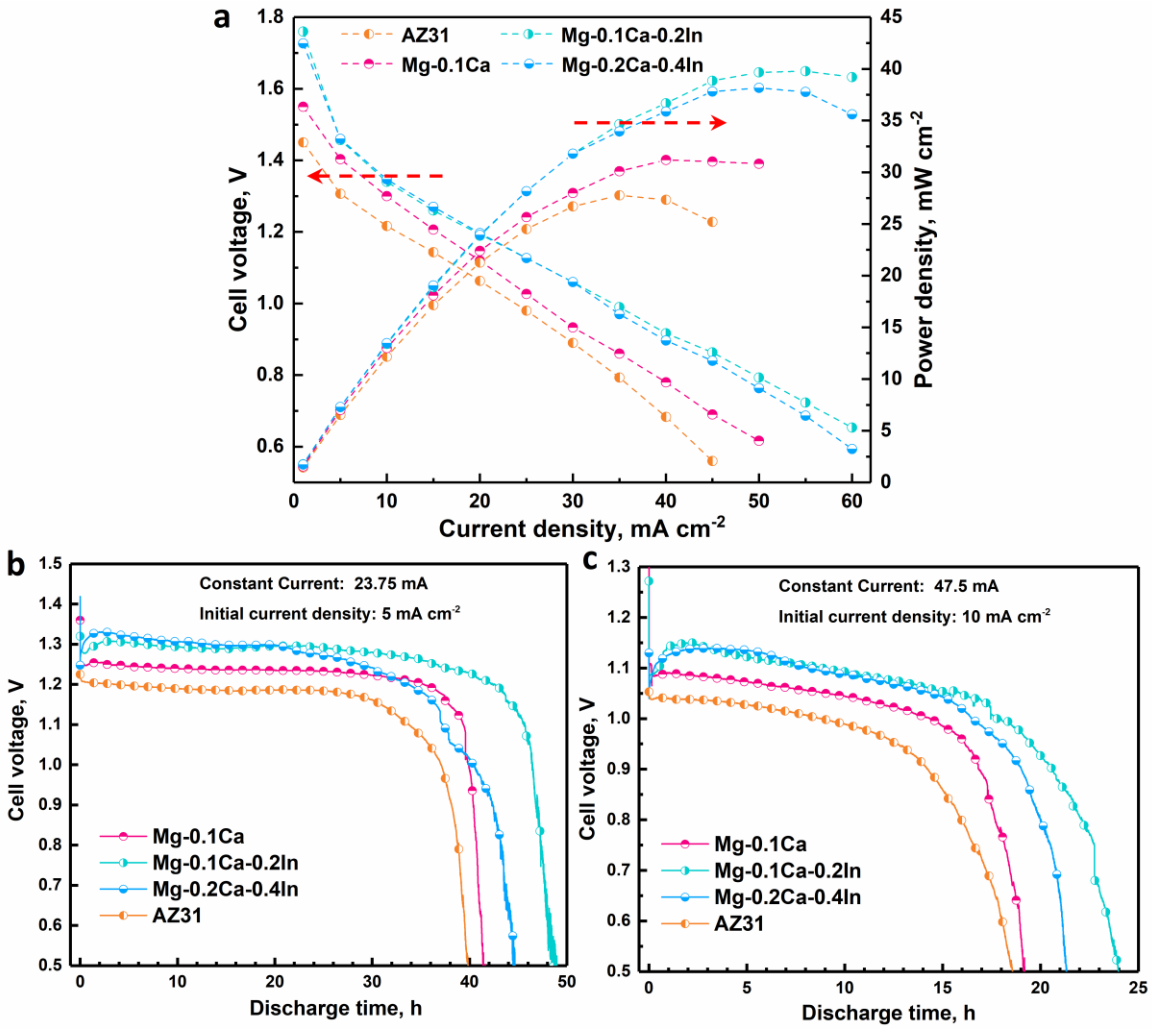

Fig. 8. (a) Cell voltage and power density of a lab-made Mg-air cell at different current densities adopting diverse Mg anodes. Average of three measurements is presented. (b, c) Voltage profiles of the Mg-air cell during the battery discharge tests applied with different current load. The adopted electrolyte is 3.5 wt.% NaCl solution, while the cathode is a commercial air cathode with C/MnO_2 catalysts

In conclusion, micro alloying with indium can improve the properties of Mg-Ca anode and, thus, boost the cell voltage and energy density of Mg-air system. Mg-0.2Ca-0.4In anode renders similar discharge voltage to Mg-0.1Ca-0.2In but the anodic efficiency is slightly lower. Therefore, Mg-0.1Ca-0.2In is suggested herein as an excellent anode material enabling superior voltage and energy density for primary Mg-air batteries. The proposed strategy, i.e. micro alloying with Ca/In, is feasible for improving anode properties and, thus, achieving high performance Mg-air batteries.

Table 3. Battery properties of Mg-air cells assembled with varied Mg anodes obtained from the battery failure tests. Note that the capacity and energy density are only based on the mass of Mg anode. Mean of data obtained from two independent measurements, which show a deviation below 5%, is presented.

Current drain	parameters	Mg-0.1Ca	Mg-0.1Ca-0.2In	Mg-0.2Ca-0.4In	AZ31
23.75 mA	Service life, h	40.6	49.1	44.4	39.2
	Anodic efficiency, %	66.4	80.2	72.6	62.7
	Capacity, mA h g^{-1}	1482	1791	1621	1405
	Average voltage, V	1.21	1.26	1.24	1.14
	Energy density, Wh kg^{-1}	1835	2259	2011	1629
47.5 mA	Service life, h	19.2	24.0	21.3	18.6
	Anodic efficiency, %	61.9	77.8	68.3	60.6
	Capacity, mA h g^{-1}	1380	1736	1524	1354
	Average voltage, V	0.99	1.04	1.06	0.93
	Energy density, Wh kg^{-1}	1378	1808	1612	1282

4. CONCLUSIONS

Herein, we propose micro alloying Mg anode with the combination of Ca/In as a feasible strategy to improve the battery properties of primary Mg-air system. Two micro-alloyed Mg anodes, i.e., Mg -0.1%Ca -0.2%In and Mg -0.2%Ca -0.4%In (weight percent hereafter), are fabricated and evaluated in terms of corrosion performance, wasteful-discharge rate and discharge activity. The addition of trace In significantly improves the discharge activity and suppresses the wasteful-discharge rate of newly developed Mg -0.1%Ca anode [30]. Moreover, the Mg-Ca-In anodes exhibit significantly lower wasteful-discharge rate than commercially accepted Mg anodes, like high purity Mg, AZ31 and AM50.

The activation of Mg anodes induced by In is based on the re-deposition of metallic In on anode surface via continuous In^{3+} ions generation accompanying anode dissolution. The re-deposited In promotes the dissolution of anode substrate via galvanic coupling with Mg and ruptures the film structure as well, leading to lower transport overpotential. The suppressed wasteful-discharge after In addition is associated with the inhibited NDE, with further mechanism remaining unclear. Consequently, Mg-air battery tests indicate that the adoption of Mg -0.1%Ca -0.2%In enables the cell to exhibit enhanced voltage and power density, compared with the cell based on AZ31 and Mg -0.1%Ca. Additionally, the battery service life is increased by using Mg-Ca-In anodes because of the boosted anodic efficiency, such as from 40.6 to 49.1 hours after replacing Mg -0.1%Ca with Mg -0.1%Ca -0.2%In at 23.75 mA current load.

Owing to the enhanced voltage and anodic efficiency, outstanding energy density is achieved via utilizing the Mg -0.1%Ca -0.2%In anode. Under 23.75 mA current load, the Mg -0.1%Ca -0.2%In-based Mg-air system exhibits an energy density of 2259 Wh kg^{-1}, which is much higher than that of a primary Zn-air (>700 Wh kg^{-1} as reported by Li et al. [64]). Therefore, with the results presented in this work, we recommend micro-alloyed Mg-Ca-In alloys, like Mg -0.1%Ca -0.2%In, as excellent candidates for anode materials of primary aqueous Mg-air batteries.

ACKNOWLEDGEMENT

Bahram Vaghefinazari is sincerely acknowledged for the discussion on experimental results. M. Deng, L. Wang and P. Jiang are grateful for the support from China Scholarship Council concerning the award of fellowship No. 201606370031, No. 201706370183 and No. 201606310043. D. Snihirova acknowledges Humboldt foundation for Postdoctoral grant and SeaMag project for financial support (MarTera ERA-NET cofund).

REFERENCES

[1] David Linden, T.B. Reddy, Handbook of Batteries, McGraw-Hill, New York, 2002.

[2] C Daniel, J. Besenhard, Handbook of Battery Materials, Wiley-VCH, Weinheim, 2012.

[3] F. Cheng, J. Chen, Chem. Soc. Rev. , 41 (2012) 2172-2192.

[4] T. Zhang, Z. Tao, J. Chen, Mater. Horiz., 1 (2014) 196-206.

[5] Md. Rahman, X. Wang, C. Wen, J. Electrochem. Soc. , 160 (2013) A1759-A1771.

[6] M. Deng, D. Höche, D. Snihirova, L.Q. Wang, B. Vaghefinazari, S.V. Lamaka, M.L. Zheludkevich, Aqueous Mg batteries, in: M. Fichtner (Ed.) Magnesium Batteries: Research and Applications, Royal Society of Chemistry, United Kingdom, 2019, pp. 275-308.

[7] R. Udhayan, N. Muniyandi, P.B. mathur, British Corroison Journal, 27 (1992) 68-71.

[8] D. Höche, S.V. Lamaka, B. Vaghefinazari, T. Braun, R.P. Petrauskas, M. Fichtner, M.L. Zheludkevich, Sci Rep, 8 (2018) 7578.

[9] Y. Li, J. Ma, G. Wang, F. Ren, Y. Zhu, Y. Song, J. Electrochem. Soc. , 165 (2018) A1713-A1717.

[10] M. Shinohara, E. Araki, M. Mochizuki, T. Kanazawa, K. Suyehiro, J. Power Sources 187 (2009) 253-260.

[11] R. Hahn, J. Mainert, F. Glaw, K.D. Lang, J. Power Sources 288 (2015) 26-35.

[12] G.L. Song, A. Atrens, Advanced Enginnering Materials, 1 (1999) 11-33.

[13] S. Thomas, N.V. Medhekar, G.S. Frankel, N. Birbilis, Curr. Opin. Solid State Mater. Sci. , 19 (2015) 85-94.

[14] T.R. Thomaz, C.R. Weber, T. Pelegrini, L.F.P. Dick, G. Knörnschild, Corros. Sci. , 52 (2010) 2235-2243.

[15] B.V. Ratnakumar, J. Appl. Electrochem. , 18 (1988) 268-279.

[16] M. Yuasa, X. Huang, K. Suzuki, M. Mabuchi, Y. Chino, J. Power Sources 297 (2015) 449-456.

[17] T. Zheng, Y. Hu, Y. Zhang, S. Yang, F. Pan, Materials & Design, 137 (2018) 245-255.

[18] L.Q. Wang, R.C. Wang, Y. Feng, M. Deng, N.G. Wang, J. Electrochem. Soc. , 164 (2017) A438-A446.

[19] K. Gusieva, C.H.J. Davies, J.R. Scully, N. Birbilis, Int. Mater. Rev. , 60 (2014) 169-194.

[20] X. Liu, S. Liu, J. Xue, J. Power Sources 396 (2018) 667-674.

[21] Y. Shi, C. Peng, Y. Feng, R. Wang, N. Wang, Materials & Design, 124 (2017) 24-33.

[22] J. Li, B. Zhang, Q. Wei, N. Wang, B. Hou, Electrochim. Acta 238 (2017) 156-167.

[23] G. Huang, Y. Zhao, Y. Wang, H. Zhang, F. Pan, Mater. Lett. , 113 (2013) 46-49.

[24] Y. Feng, W. Xiong, J. Zhang, R. Wang, N. Wang, Journal of Materials Chemistry A, 4 (2016) 8658-8668.

[25] Y. Lv, Y. Xu, D. Cao, J. Power Sources 196 (2011) 8809-8814.

[26] Y. Feng, R.-c. Wang, K. Yu, C.-Q. Peng, W.-x. Li, Transactions of Nonferrous Metals Society of China, 17 (2007) 1363-1366.

[27] Y. Feng, R. Wang, K. Yu, C. Peng, J. Zhang, C. Zhang, J. Alloys Compd. , 473 (2009) 215-219.

[28] J. Zhao, K. Yu, Y. Hu, S. Li, X. Tan, F. Chen, Z. Yu, Electrochim. Acta 56 (2011) 8224-8231.

[29] M. Deng, L. Wang, D. Höche, S.V. Lamaka, D. Snihirova, B. Vaghefinazari, M.L. Zheludkevich, J. Power Sources 441 (2019) 227201.

[30] M. Deng, D. Höche, S.V. Lamaka, D. Snihirova, M.L. Zheludkevich, J. Power Sources 396 (2018) 109-118.

[31] M. Deng, D. Höche, S.V. Lamaka, L. Wang, M.L. Zheludkevich, Corros. Sci. , 153 (2019) 225-235.

[32] H.A.E. SHAYEB, F.M.A.E. WAHAB, S.Z.E. ABEDIN, J. Appl. Electrochem. , 29 (1999) 601-609.

[33] M. Pourgharibshahi, P. Lambert, Mater. Corros. , 67 (2016) 857-866.

[34] J.B. Bessone, D.O. Flamini, S.B. Saidman, Corros. Sci. , 47 (2005) 95-105.

[35] D.O. Flamini, S.B. Saidman, Mater. Chem. Phys. , 136 (2012) 103-111.

[36] I.-J. Park, S.-R. Choi, J.-G. Kim, J. Power Sources 357 (2017) 47-55.

[37] N. Wang, R. Wang, C. Peng, B. Peng, Y. Feng, C. Hu, Electrochim. Acta 149 (2014) 193-205.

[38] S. Yuan, H. Lu, Z. Sun, L. Fan, X. Zhu, W. Zhang, J. Electrochem. Soc. , 163 (2016) A1181-A1187.

[39] X. Li, H. Lu, S. Yuan, J. Bai, J. Wang, Y. Cao, Q. Hong, J. Electrochem. Soc. , 164 (2017) A3131-A3137.

[40] A. Pardo, M.C. Merino, A.E. Coy, F. Viejo, R. Arrabal, S. Feliú, Electrochim. Acta 53 (2008) 7890-7902.

[41] K.A. Unocic, H.H. Elsentriecy, M.P. Brady, H.M.M. III, G.L. Song, M. Fayek, R.A. Meisner, B. Davis, J. Electrochem. Soc. , 161 (2014) C302-C311.

[42] N.-g. Wang, R.-c. Wang, C.-q. Peng, Y. Feng, X.-y. Zhang, Transactions of Nonferrous Metals Society of China, 20 (2010) 1403-1411.

[43] P. Gore, S. Fajardo, N. Birbilis, G.S. Frankel, V.S. Raja, Electrochim. Acta 293 (2019) 199-210.

[44] D. Hoche, C. Blawert, S.V. Lamaka, N. Scharnagl, C. Mendis, M.L. Zheludkevich, Phys. Chem. Chem. Phys. , 18 (2016) 1279-1291.

[45] S.V. Lamaka, D. Höche, R.P. Petrauskas, C. Blawert, M.L. Zheludkevich, Electrochem. Commun. , 62 (2016) 5-8.

[46] S.V. Lamaka, B. Vaghefinazari, D. Mei, R.P. Petrauskas, D. Höche, M.L. Zheludkevich, Corros. Sci. , 128 (2017) 224-240.

[47] S. Fajardo, G.S. Frankel, Electrochim. Acta 165 (2015) 255-267.

[48] G.L. Song, A. Atrens, D. StJohn, Magnesium Technology, (2001) 255-262.

[49] M. Esmaily, J.E. Svensson, S. Fajardo, N. Birbilis, G.S. Frankel, S. Virtanen, R. Arrabal, S. Thomas, L.G. Johansson, Prog. Mater Sci. , 89 (2017) 92-193.

[50] Y. Jin, C. Blawert, F. Feyerabend, J. Bohlen, M. Silva Campos, S. Gavras, B. Wiese, D. Mei, M. Deng, H. Yang, R. Willumeit-Römer, Corros. Sci. , 158 (2019) 108096.

[51] C.L. Mendis, K. Oh-ishi, T. Ohkubo, K. Hono, Scr. Mater. , 64 (2011) 137-140.

[52] H. Xie, H. Pan, Y. Ren, L. Wang, Y. He, X. Qi, G. Qin, Phys. Rev. Lett. , 120 (2018) 085701.

[53] A.W.C. Lin, N.R. Armstrong, T. Kuwana, Anal. Chem. , 49 (2002) 1228-1235.

[54] M. Faur, M. Faur, D.T. Jayne, M. Goradia, C. Goradia, Surf. Interface Anal. , 15 (1990) 641-650.

[55] S. Yuan, H. Lu, Z. Sun, L. Fan, X. Zhu, W. Zhang, J. Electrochem. Soc. , 163 (2016) A1181-A1187.

[56] Z. Qiao, Z. Shi, N. Hort, N.I. Zainal Abidin, A. Atrens, Corros. Sci. , 61 (2012) 185-207.

[57] F. Cao, Z. Shi, G.-L. Song, M. Liu, A. Atrens, Corros. Sci. , 76 (2013) 60-97.

[58] M. Liu, P.J. Uggowitzer, A.V. Nagasekhar, P. Schmutz, M. Easton, G.-L. Song, A. Atrens, Corros. Sci. , 51 (2009) 602-619.

[59] P. Jiang, C. Blawert, R. Hou, N. Scharnagl, J. Bohlen, M.L. Zheludkevich, J. Alloys Compd. , 783 (2019) 179-192.

[60] S. Fajardo, C.F. Glover, G. Williams, G.S. Frankel, Electrochim. Acta 212 (2016) 510-521.

[61] G.S. Frankel, A. Samaniego, N. Birbilis, Corros. Sci. , 70 (2013) 104-111.

[62] G.G. Perrault, Electroanlytical Chemistry of The Magnesium Electrode In Aqueous Solution, 27 (1970) 47-58.

[63] C.D. Taylor, J. Electrochem. Soc. , 163 (2016) C602-C608.

[64] Y. Li, M. Gong, Y. Liang, J. Feng, J.E. Kim, H. Wang, G. Hong, B. Zhang, H. Dai, Nat Commun, 4 (2013) 1805.